ELSEVIER

J. Non-Newtonian Fluid Mech. 102 (2002) 361–382

Journal of Non-Newtonian Fluid Mechanics

www.elsevier.com/locate/jnnfm

The shear flow behavior of LCPs based on a generalized Doi model with distortional elasticity

G. Sgalari [a,*], G.L. Leal [a], J.J. Feng [b]

[a] *Department of Chemical Engineering, University of California, Santa Barbara, CA, USA*

[b] *The Levich Institute for Physicochemical Hydrodynamics, City College of the City University of New York, New York, NY, USA*

Abstract

We consider the shear flow behavior of nematic LCPs, modeled via an extension of the Doi theory that incorporates the mean-field nematic potential due to Marrucci and Greco to account for distortional elasticity. Based upon the constitutive model that derives from this starting point, we utilize finite-element methods to investigate the LCP behavior in a planar shear flow. We assume that the LCP is pinned at the walls and is initially in its equilibrium configuration. The goal of our simulations is to explore the evolution of the LCP structure and the flow. Our results show that in-plane tumbling instabilities lead to a non-uniform orientation field, which, in turn, arrests tumbling. The resulting quasi-steady-state texture is characterized by a length scale that seems to be consistent with a Marrucci-like scaling. When we allow for out-of-plane tipping of the director, we predict an out-of-plane director instability, which is qualitatively consistent with what has been observed in experiments.

Keywords: Liquid crystal polymers; Distortional elasticity; Tumbling; Disclinations; Texture

1. Introduction

There has been a long history of scientific interest in liquid crystalline polymers (LCPs), but relatively few technological applications other than high tensile strength fibers, such as Kevlar. This is due to the intrinsic difficulty of maintaining a monodomain orientational state at the macroscopic level, or at least of controlling the microstructural orientation state in any processing flow other than fiber spinning. When a nematic LCP undergoes a processing flow that involves a dominant component of shear (e.g. flow into a mold), there is an immediate formation and/or proliferation of singular structures (points or lines), known as disclinations, in the orientation field. This leads, generally, to a polydomain structure of randomly oriented nematic microdomains (i.e. regions with nearly uniform orientation), and thus, to a material whose rheological and optical properties are largely those of an ordinary isotropic polymer. Since this

* Corresponding author.

E-mail address: gio@engineering.ucsb.edu (G. Sgalari).

Dedicated to Professor Acrivos on the occasion of his retirement from the Levich Institute and the CCNY.

0377-0257/02/$ – see front matter
PII: S0377-0257(01)00187-2

does not occur in the extensional motion of fiber spinning, we may conclude that the nature of the flow is an important factor in determining the material microstructure. We know moreover that the tumbling nature of LCPs is crucial for the appearance of the above-mentioned cascade of flow instabilities. In particular, disclinations are much less common in small-molecule nematics, which in general adopt a fixed orientation near the flow direction when subject to shear flow. In polymeric LCPs, on the other hand, the average direction of orientation almost always rotates continuously in a shearing flow (they exhibit "tumbling" behavior). However, a complete understanding of the dynamics of texture evolution and its interaction with the flow, which is of crucial importance to any future development of LCPs as structural materials, is still missing.

Many experimental investigations have been dedicated to the study of this problem, the most comprehensive of which are the two papers by Larson and Mead [1,2]. They studied the textural evolution of a typical LCP solution (PBG) during planar steady shear for a wide range of parameter values and for different anchoring conditions. Even in such a simple geometry they found that the material exhibits a very rich microstructural/rheological behavior with multiple transitions in texture. Their main findings, which are summarized below, are schematically illustrated in Fig. 1. For parallel and homeotropic BCs the director tips out of the shear plane and the system undergoes a first textural transition with the formation of a pattern of bands perpendicular to the flow. At later times, the material exhibits a second transition with the formation of stripes parallel to the flow direction.

The final striped pattern has been quantitatively characterized by later works (e.g. [3,4]). Still limited, however, is the number of observations of the transient banded texture at intermediate times [5], which is not to be confused with the banded structure that appears after cessation of shear.

Several attempts to analyze these experimental observations have been made via numerical calculations using the Leslie–Ericksen (LE) theory. We may recall that the basic assumptions of the LE theory require slow flows and weak distortions (i.e. conditions in which the director rotates but the shape of the orientation distribution is unperturbed from its equilibrium form). The 2D flow simulations of Han and Rey [6–8] were able to capture the instability that drives the average orientation—which is often associated with a unit vector known as the *director*—out of the shear plane and then leads to a banded texture similar to that observed in experiments. However, because they used the LE theory, their calculations are relevant only for low values of the shear rate and their results cannot be expected to hold quantitatively, or possibly

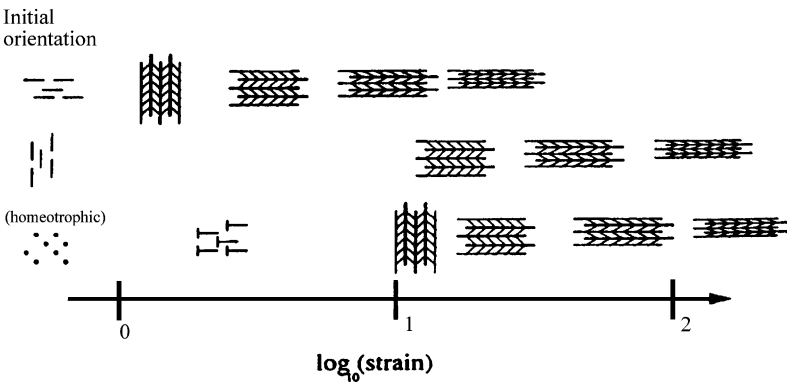

Fig. 1. Typical textural evolution of an LCP solution (PBG-198) during shear [2].

even qualitatively, at the higher values of shear rate found in processing flows. Recent simulations by Feng et al. [9], also done in the LE context, allowed for gradients in the vorticity direction rather than the flow direction, and thus were able to capture the secondary flow instability that produces roll cells and orientation patterns that can be related to the final striped texture of real materials (since no gradients were allowed in the flow direction, the banded instability previously mentioned could not be observed). Most interestingly, this latter work provided a suggestion for a detailed mechanism of disclination formation, which leads to "thick", coreless defect lines that are associated with the roll cell boundaries. The use of the LE theory, however, again limits the range of validity of these predictions. In particular, it leaves out the potentially critical viscoelastic effects due to distortion of the orientation distribution, which are an essential characteristic of the other type of defect that characterizes real systems, i.e. "thin" disclinations with a core in which the orientational order is much lower than at equilibrium [10]. We believe therefore that a consistent treatment of defect formation leading to quantitative predictions of the rheological behavior of LCPs is obtainable only in the context of a molecular theory that incorporates both "distortional elasticity" due to spatial gradients of the configuration field and "viscoelasticity" due to distortions in the shape of the distribution function.

For this purpose, the original molecular model due to Doi is incomplete as it includes viscoelasticity but does not incorporate distortional elasticity. An attempt to overcome this limitation of the Doi theory was made by Larson and Doi [11] with the formulation of an ad hoc mesoscopic model. This model combined the original Doi theory, which is valid for a monodomain nematic, with phenomenological equations for the evolution of the various microdomains. However, it provides only qualitative indications of expected scaling laws and overall stresses, and cannot predict the details of the microstructural evolution of LCPs.

A breakthrough came in recent years with a workable proposal by Marrucci and Greco [12] for the incorporation of long-range distortional elasticity into the Doi model via a generalization of the Maier–Saupe mean-field potential. Their expression for this mean-field potential was recently incorporated into a new constitutive theory that is appropriate for flow analysis of LCPs [13]. Earlier models proposed by Tsuj and Rey [14] and by Kupfermann et al. [15] either neglected the coupling between the microstructural state and the stress field [14], or were missing important terms in the expression for the elastic stress [15].

In the present paper, we use the full model developed by Feng et al. [13] for 2D flow simulations of LCPs. Our report begins with a brief review of the theoretical framework, the details of which can be found in the original reference, and with a discussion of the most important aspects of our numerical scheme. We then present two sets of detailed results for planar shear flows. In the first, we assume that the configuration tensor is symmetric with respect to the plane of shear (i.e. its three eigenvectors lie either in the plane of shear or perpendicular to it). These results show the emergence of a texture that is characterized by a specific length scale. The dependence of this length scale on the relevant parameters is analyzed and compared with a generalization of the scaling proposed by Marrucci [16]. This first series of results is also directly comparable to the only previous numerical work with full coupling between structure and stress [15]. Kupfermann's work is characterized by the dual assumptions of a 1D flow (this choice made irrelevant the missing term in the stress expression they used) and a 2D configuration tensor (i.e. they assumed that all molecules lie in the plane of shear). A puzzling result was that their solutions did not show evidence of the expected scaling behavior. The first part of the present work is thus focused on a reexamination of this issue.

In the second part of the paper, we remove the symmetry constraint on the molecular orientation. In other words, we allow for a fully 3D configuration tensor, though still with the assumption that the flow is 2D. This precludes the possibility of predicting roll-cell formation, but does allow the prediction of

the out-of-plane director tipping which has been associated with the transient banded pattern observed in experiments [1,2,8]. We then conclude with a preliminary evaluation of the predictive capabilities of our theoretical model.

2. The theoretical model

The model used in this study is an extension of the Doi theory for nematic polymers. Like the Doi theory, it is based on a statistical mechanics description of a suspension of rigid rod-like molecules. This model takes into account the effects of flow, Brownian motion and intermolecular forces (both local and non-local) on the molecular orientation distribution. Assuming the number density of polymer molecules is constant in space, the kinetic equation governing the evolution of the polymer configuration is written as:

$$\frac{D\Psi}{Dt} = -\boldsymbol{u} \times \frac{\partial}{\partial \boldsymbol{u}}[\boldsymbol{u} \times \nabla \boldsymbol{v}^{\mathrm{T}} \boldsymbol{u} \Psi] + D_{\mathrm{r}} \frac{\partial}{\partial \boldsymbol{u}} \left[\frac{\partial \Psi}{\partial \boldsymbol{u}} + \Psi \frac{\partial}{\partial \boldsymbol{u}} \left(\frac{V}{kT} \right) \right] \tag{1}$$

Here $\boldsymbol{u}$ is a unit vector specifying the orientation of a rod, Ψ the orientation distribution function, $\boldsymbol{v}$ the macroscopic velocity, D_{r} the rotational diffusion coefficient and V is the mean-field nematic potential. The most significant difference from the original Doi theory is the replacement of the Maier–Saupe potential with the Marrucci–Greco potential [12]:

$$V(\boldsymbol{u}) = -\frac{3kT}{2} U \left(\boldsymbol{S} + \frac{l^2}{24} \nabla^2 \boldsymbol{S} \right) : \boldsymbol{uu} \tag{2}$$

Here the so-called configuration tensor, $\boldsymbol{S}$, is the second moment of Ψ, while U specifies the strength of the nematic potential and l is a length scale that is characteristic of distortional elasticity. This form for the nematic potential takes account of the energy penalty due to a "gradually varying" orientation field, the non-local elasticity neglected by Doi.

We shall see that the stress tensor is expressed in terms of moments of Ψ. Hence, rather than solve Eq. (1), the numerical calculations are based on the solution of an approximate equation for $\boldsymbol{S}$, which is derived from Eq. (1) by multiplying both sides by $\boldsymbol{uu}$ and integrating over the configuration space (i.e. the unit sphere). In dimensionless form the resulting equation reads:

$$\frac{D\boldsymbol{S}}{Dt} = -2\boldsymbol{D} : \boldsymbol{Q} - \frac{f}{De} \left(\boldsymbol{S} - \frac{\boldsymbol{I}}{3} \right) + \frac{Uf}{De} \left(\boldsymbol{SS} - \boldsymbol{S} : \boldsymbol{Q} + \frac{1}{48} \left(\frac{l}{L} \right)^2 (\nabla^2 \boldsymbol{SS} + \boldsymbol{S} \nabla^2 \boldsymbol{S} - \nabla^2 \boldsymbol{S} : \boldsymbol{Q}) \right) \tag{3}$$

where $\boldsymbol{D}$ is the symmetric part of the velocity gradient tensor, $\boldsymbol{Q}$ the fourth moment of Ψ, L the length scale characteristic of the macroscopic flow, De the Deborah number defined as $\dot{\gamma}/6D_{\mathrm{r0}}$ [1] (D_{r0} is the rotational diffusivity of an isotropic suspension having the same number density of molecules) and $f = (1 - \boldsymbol{S} : \boldsymbol{S})^{-2}$. This last function was proposed by Doi [17], to account for the dependence of the

[1] The Deborah number is usually defined as the ratio of the time scales of molecular diffusion and flow, i.e. $\dot{\gamma}/\bar{D}_{\mathrm{r}}$. In our system, such a quantity varies with position, because of the dependence of the average orientational diffusivity on the local value of the order parameter (expressed in Eq. (4)). The particular grouping we choose to define De has the same qualitative significance as $\dot{\gamma}/\bar{D}_{\mathrm{r}}$, but is independent of position, and proves also to provide a convenient form for the resulting equations.

rotational diffusivity on the molecular configuration, i.e. the average rotational diffusivity is assumed to be:

$$\bar{D}_{\mathrm{r}} = D_{\mathrm{r}0} f = \frac{D_{\mathrm{r}0}}{(1 - \boldsymbol{S} : \boldsymbol{S})^2} \tag{4}$$

It is important to note that $\boldsymbol{Q}$ has to be expressed in terms of $\boldsymbol{S}$ via closure approximations for Eq. (3) to be self-contained. Previous work on theoretical aspects of the closure problem [18–20] has shown that the best approach is a mixed treatment where the viscous term $\boldsymbol{D}$:$\boldsymbol{Q}$ is closed via the so-called Bingham closure [18], while the remaining elastic terms $\boldsymbol{S}$:$\boldsymbol{Q}$ and $\nabla^2\boldsymbol{S}$:$\boldsymbol{Q}$ are closed via the quadratic closure (i.e. $\boldsymbol{Q} = \boldsymbol{SS}$). This choice allows for a numerically manageable implementation, while preserving director tumbling, which exists in the solutions of the unapproximated Eq. (1) and is the key to understanding the origin of disclinations in flow (i.e. tumbling solutions are suppressed if the quadratic closure is used for the viscous term as well).

The other essential feature of the present model is the governing equation for the stress. Following the notation of Doi and Edwards [21], the stress is divided into a viscous and an elastic part. The viscous stress is the same as in the original Doi theory, while the expression for the elastic component has to be modified to account for distortional elasticity. The procedure to accomplish this is shown in [13] and we report here only the resulting expression for the total stress:

$$\sigma = \frac{De}{\beta}\boldsymbol{D} : \boldsymbol{Q} + \boldsymbol{S} - U\left[(\boldsymbol{SS} - \boldsymbol{Q} : \boldsymbol{S}) - \frac{1}{24}\left(\frac{l}{L}\right)^2\left(\boldsymbol{Q} : \nabla^2\boldsymbol{S} - \boldsymbol{S}\nabla^2\boldsymbol{S} - \frac{\nabla\boldsymbol{S}\nabla\boldsymbol{S} - \nabla^2\boldsymbol{S} : \boldsymbol{S}}{4}\right)\right] \tag{5}$$

Here β is the square of the volumetric concentration divided by an empirical coefficient of $O(10^3)$ (see Section 9.4.3 of [21]).

We write the equation of motion as:

$$Re\frac{\partial \boldsymbol{v}}{\partial t} = -\nabla p + \nabla^2\boldsymbol{v} + \frac{c}{De}\nabla\sigma \tag{6}$$

with $c = \alpha kT/2\eta_{\mathrm{s}}D_{\mathrm{r}0}$ known as the coupling parameter, which contains the solvent viscosity η_{s} and the number density of polymer molecules α. Since we considered low Reynolds flows, we neglected the nonlinear term $\boldsymbol{v}\nabla\boldsymbol{v}$. Although we kept the $\partial\boldsymbol{v}/\partial t$ to make evident the transient nature of the problem, this term is also small and the choice to keep it is mainly historical.

3. The problem set-up

3.1. The geometry of the system

The problem we analyze here is the model LCP described in the previous section, undergoing a traction-driven shear flow between two plane parallel boundaries. We assume that the various independent variables (i.e. velocity, pressure and structure tensor) may be functions of two spatial coordinates: x and y, which are the flow and shear gradient directions, respectively. We include the variation along the flow direction, instead of considering a simple 1D shear flow, because, in the second part of the work, we hope to predict configuration fields that could be related to the banded pattern that is periodic along the flow

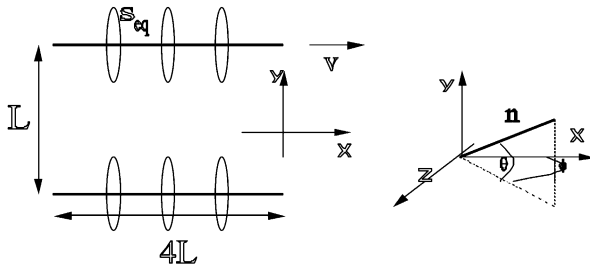

Fig. 2. System geometry with homeotropic BC and angles defining the director (i.e. the major eigenvector of the structure tensor).

direction, and observed in real sheared LCPs. On the other hand, we limit the flow to 2D for this initial study in order to reduce the size of the numerical problem. This means that we will *not* be able to simulate the final steady striped texture of real materials, due to roll cells parallel to the flow (see Fig. 2). The only previous calculations using a full viscoelastic model [15] were restricted to a 1D flow.

We consider, in particular, a region of width L in the y-direction (across the channel) and length $4L$ in the flow direction, x. Due to the limitations of memory and computation time that will be discussed when commenting on the mesh discretization, we did not consider much larger boxes and we cannot exclude, therefore, the possibility that size effects might affect the results of our simulations. We believe, nevertheless, that the aspect ratio chosen is a reasonable compromise between the need for a long enough computational domain to reduce the influence of the inflow and outflow boundaries and the numerical limitations, and that the qualitative features of the predictions would not be modified by the choice of larger domains Fig. 2.

We prescribe the value of the velocity at the top and bottom walls, and assume periodic BCs for the inflow–outflow boundaries (for detailed comments on the issue of BCs for transient non-homogenous flows of LCPs (see [22]). We assume either *homeotropic* or *parallel anchoring* at the walls implying that the average orientation is either normal or parallel to the walls with the order parameter $s = ((3\boldsymbol{S} : \boldsymbol{S} - 1)/2)^{1/2}$ at its equilibrium value. Finally, we assume that the system is initially at rest with a uniform equilibrium configuration, with the orientation determined by the prescribed anchoring conditions at the walls.

We consider the orientation distribution to be fully 3D. In other words while we consider the flow to be restricted to the plane of shear, we allow molecules to be oriented out of the shear plane. This difference in the dimensionality between the flow geometry and the orientation space is due to our desire to capture the out-of-plane orientation instability that drives the first textural transition of real systems, as previously mentioned.

In the first half of the work, we assume that the configuration tensor is symmetric with respect to the plane of shear (i.e. its three eigenvectors either lie in the plane of flow or are perpendicular to it or, equivalently, S_{xz} and S_{yz} are 0). This choice simplifies the calculations and strongly reduces the required computation time and memory space. It thus seems a reasonable assumption for a preliminary analysis of the performance of our scheme. In fact, since it is generally agreed that the cause of texture development is the tumbling nature of LCPs, the in-plane evolution of the director is the first essential aspect of the system to monitor. This simplifying assumption also makes it possible to compare our results with the work of Kupfermann et al. [15]. We note that the assumption in their work was actually even more restrictive as they constrained all molecules to be in the shear-plane, considering in other words only an in-plane 2D configuration tensor with S_{xz}, S_{yz} and S_{zz} all set to 0.

In the second part of this paper, the symmetry constraint on the director orientation is removed in order to take the first step toward a more realistic system that will allow meaningful comparisons with experimentally observed textures.

3.2. Choice of parameters

An important issue, especially for comparisons between the present numerical results and experiments, is the value of the various model parameters. The coefficient β was estimated empirically by comparing the expression for the viscous stress (Eq. (5)) to experimental data for LCP solutions [23,24] and was thus set to 2000. A check was made that varying the value of β in the range 200–20,000 did not substantially modify the qualitative behavior of the solution. Reducing β had only the effect of slowing down the tumbling-suppression process. A reduction of the value of β corresponds in fact to a reduction of the magnitude of anchoring effects relatively to the flow. The coupling parameter c was fixed at 100. This value is slightly lower than what is expected in real systems. However, it allowed us to achieve convergence of the numerical scheme without having to resort to special techniques for the solution of the full set of equations (i.e. the time stepping was done by a simple sequential solution of the flow and configuration equations).

The strength of the nematic potential U was varied in the range 6–10 and, for reasons that we will explain in a following section, these values of U led to a corresponding range of De from 5 to 30. The ratio l/L was varied in the range $[0.5\text{–}4] \times 10^{-3}$, so that the Ericksen number, which is defined as $Er = (L/l)^2(De/U)$, was in the range $Er \approx 10^6$–10^7. This choice for the Er and De allowed us to make a comparison with the work on PBG solutions [1] (these values constitute the upper end of the spectrum they studied experimentally).

The Reynolds number was fixed at 10^{-2}. As previously said, a small non-zero value of the Reynolds number was chosen to make evident the transient nature of the flow problem. The inertial term is in fact negligible when compared to the other terms in Eq. (6) and the particular value of the Re used affects only the number of iterations required by the inner stokes solver at each time step.

4. The numerical algorithm

To simulate planar non-homogenous flows of LCPs with distortional elasticity, we extended the finite-element code for viscoelastic flows that was first developed by Singh and Leal [25]. The algorithm had been successfully applied, in previous studies, to the simulation of transient flows of LCPs using the original Doi theory [22,26,27] and needed only modest modifications for the implementation of the additional long-range elastic terms. This implementation is based on a linearized version of Eq. (3), which, at every time step, is solved iteratively:

$$\begin{aligned}\frac{\boldsymbol{S}^i - \boldsymbol{S}^0}{\Delta t} = {} & -2\boldsymbol{D} : \boldsymbol{Q}^i_{\text{bingham}} - \frac{1}{De}\left(\boldsymbol{S}^i - \frac{\boldsymbol{I}}{3}\right)\boldsymbol{S} \\ & - \frac{U}{De}\left((\boldsymbol{S}^{i-1} : \boldsymbol{S}^{i-1})\boldsymbol{S}^i + \frac{1}{48}\left(\frac{l}{L}\right)^2 (\nabla^2 \boldsymbol{S}^{i-1} : \boldsymbol{S}^{i-1})\boldsymbol{S}^i\right)\frac{U}{De} \\ & \times \left(\boldsymbol{S}^{i-1}\boldsymbol{S}^{i-1} + \frac{1}{48}\left(\frac{l}{L}\right)^2 (\nabla^2 \boldsymbol{S}^{i-1}\boldsymbol{S}^{i-1} + \boldsymbol{S}^{i-1}\nabla^2 \boldsymbol{S}^{i-1})\right) \end{aligned} \tag{7}$$

Here the superscript indicates the iteration number, and $\boldsymbol{S}^0$ is the configuration tensor at the previous time step. The linearization chosen treats the Laplacian terms explicitily so that an iterative solver is needed to ensure the continuity of the solution near the walls. The dirichlet BC on the walls are, in fact, ensured, at each iteration, by the penalty method. The small value of the parameter l/L in our system and the fine discretization near the boundaries make this scheme quickly convergent. Moreover, even with the explicit treatment of the second order derivative, we did not observe any of the instabilities that prompted the development of the EVSS-G/FEM by Szady et al. [28] for viscoelastic flow with a hyperbolic constitutive equation near no-slip surfaces, nor those that characterize systems with a constitutive equation that changes type, as in Joseph and Saut [29].

Eq. (7) is solved in the frame of reference defined by the local principal axes of $\boldsymbol{S}^0$, because this allows for an easier implementation of both the Bingham closure and Patankar's algorithm to ensure the non-negative definiteness of $\boldsymbol{S}$ (details of this numerical feature are given in Singh and Leal [25]). In the finite-element formulation we used, with the Laplacian terms treated explicitly, Eq. (7) results in a set of linear equations with a diagonal matrix of coefficients of half-bandwidth 5 (due to symmetry and the constraint $\boldsymbol{S} = 1$, the configuration tensor $\boldsymbol{S}$ has only five independent components in the fully 3D case), which are solved, at each iteration, by a standard SOR solver.

An important issue addressed in the present implementation was the treatment of the Laplacian terms. Our finite-element formulation uses bilinear shape functions for the configuration tensor (we used pseudo-P2 triangular elements) and so for a meaningful evaluation of the second-order derivatives we had to devise a finite-difference formula. The formula reads:

$$\left.\frac{\partial^2 f}{\partial x^2}\right|_{x=x_0} \rightarrow \frac{-30f_0 + 16f_1 + 16f_{-1} - f_2 - f_{-2}}{12h^2} + \mathrm{O}(h^3) \tag{8}$$

The five points considered in the formula are indicated in the figure below, and the values of f at the various points are interpolated from nodal values in the appropriate element. This five point formula with third-order accuracy is consistent with the treatment adopted for the convective term (for details see [25]), one of the most praised [30] features of the original code (Fig. 3).

4.1. The finite-element mesh

Great care was taken in the construction of the mesh, especially the discretization along the shear gradient direction. As will be explained later, it is in fact along that direction that the system starts to develop a texture and therefore it is the shear-gradient discretization that plays the most critical role in

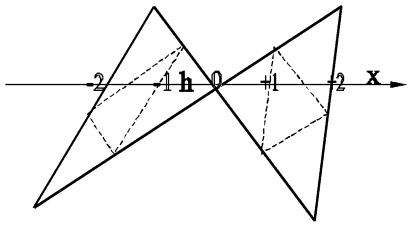

Fig. 3. Pseudo-P2 triangular elements and points for the finite-difference formula.

the accuracy of the results. We tested grids with an average of 50, 80 and 100 nodes in the shear gradient direction. The latter 2 mesh produced practically indistinguishable results for the values of the parameters chosen in our study. We also tested an 80-node grid with the nodes unevenly spaced (i.e. more closely packed near the walls) and this brought a slight improvement in the definition of the Fourier spectra peak (see Section 5.2). The non-uniformities in orientation, in fact, propagate from the region close to the wall and it is then expected that the need for an accurate discretization is greater there. This 80 unevenly-spaced nodes grid is the one actually used in the simulations.

As a last remark on the issue of mesh size, we note that we restricted our attention to a limited area of the *Er–De* parameter space. Experiments have shown that for certain values of those parameters (e.g. the last stages of the Ericksen number cascade where roll cell refinement leads to director turbulence [2]), the material becomes highly textured and simulations in those circumstances would have required a finer mesh in the shear gradient direction than the one we used. We preferred instead to analyze the 2D problem and the resulting computations were already quite "bulky". In particular, the 80 nodes in the shear-gradient direction result in a total actual number of nodes for the 2D mesh of the order of 10^4. Of course, we could not use too coarse a discretization in the flow direction compared to the one on the shear-gradient direction because strongly irregular elements would have affected the accuracy of our computations. More importantly, we wanted to be able to ensure adequate discretization to be able to capture the cross-stream banded flow structure.

5. Part I: configuration tensor symmetric with respect to shear-plane

5.1. Objective and general remarks

In this first section of results, we have considered the flow and microscale configuration under the assumption that the configuration tensor is symmetric with respect to the plane of shear. Our objective is basically to see whether our new constitutive model can predict the development of a spatial texture across the gap of the shear cell and, if so, determine how the characteristic length scale that emerges depends upon the relevant parameters. Specifically, it is of interest to determine whether the texture scale is consistent with the qualitative predictions of Marrucci [16], as outlined below, and/or is comparable to the earlier computational results of Kupfermann et al. [15]. Although the latter were obtained using a slightly flawed rheological model, the calculations were carried out for 1D shear flow, and in this case the corrected expression for the stress tensor [13] reduces to the form that they used. Thus, our calculations should be directly comparable to their results (with the exception of the more restrictive symmetry assumptions they adopted). Since their results did not scale as expected from the Marrucci argument, it is important to understand whether this is a generic deficiency in the constitutive model, or a non-applicability of the Marrucci scaling to the system analyzed (i.e. one that cannot be described by the simple LE model), or perhaps nothing more than an artifact of their numerical method, their symmetry assumptions or their choice of parameter values.

Before discussing our results, it is worthwhile to briefly review the Marrucci argument and consider how (or whether) it may be expected to apply to the present system. The Marrucci scaling is based upon the simple hypothesis, appropriate when working in the LE context, that a steady state is reached in a sheared nematic when distortional elasticity and viscous torques balance each other. If we refer to the microstructural balance in Eq. (3), we see that the ratio of the magnitude of these two forces (represented,

respectively, by the last and first terms of the right hand side) is:

$$\frac{U}{De}\left(\frac{l}{L}\right)^2 (\nabla \boldsymbol{S})^2 \tag{9}$$

Marrucci's hypothesis is that dynamically stationary states correspond to a fixed value of this ratio. To represent the order of magnitude of the gradient of the orientation non-dimensionalized with respect to the macroscopic length scale L, it is convenient to introduce a texture length scale h_{text}, defined as the characteristic length scale for changes in orientation, so that $(\nabla \boldsymbol{S})^2 \sim 1/(h_{\text{text}}/L)^2$. Substituting this into Eq. (9), we see that the Marrucci scaling requires:

$$\frac{h_{\text{text}}}{L} \propto \frac{l}{L}\left(\frac{U}{De}\right)^{1/2} \tag{10}$$

Hence, we should expect any orientational texture that develops in a flow to be directly proportional to the length scale l, and to depend on U and De in the manner shown in Eq. (10).

Although the scaling prediction Eq. (10) pertains strictly to a texture scale that develops in the shear gradient direction, it has been applied (e.g. [2]) in a loose sense to estimate the length scale of the striped texture with periodicity along the vorticity direction that emerges in real materials under shear. In the present section, however, we consider only length scales of the texture in the shear gradient direction.

When molecular elasticity is considered, as in the model used in this study, the Marrucci argument leading to Eq. (10) cannot, in general, be applied. Steady state is established as a dynamic balance between the *three* physical contributions to Eq. (3): i.e. viscous forces, gradient elasticity and molecular elasticity (or viscoelasticity). In the present work, however, we carried out a set of calculations for specially chosen pairs of values of U and De for which we may expect the scaling in Eq. (10) to apply. As shown in Fig. 4, the (U, De) points we consider are all close to the curve at which there is a transition from tumbling to wagging for the *homogenous* Doi model in linear shear flow (this curve was derived by Feng et al. [27]). This transition occurs, for a given value of the nematic strength U, at a shear rate (i.e. De) that produces a critical amount of defocusing of the orientation distribution, e.g. approximately a fixed difference between the minimum value of the order parameter $\boldsymbol{S}$ over one rotational period and the

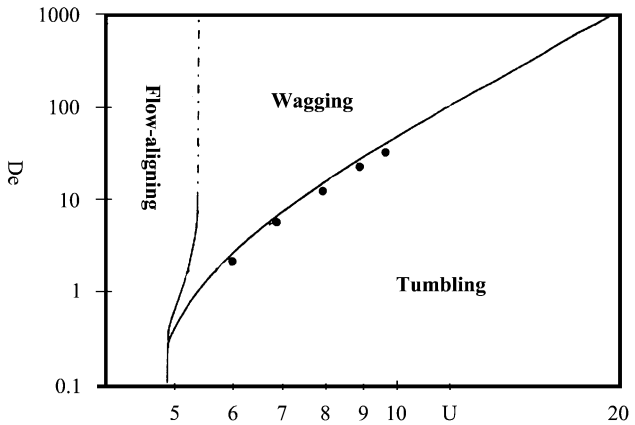

Fig. 4. Tumbling behavior transitions for the monodomain nematic. The *U–De* values used in the present work are indicated by the solid dots.

equilibrium value $\boldsymbol{S}_{\mathrm{eq}}$. Hence, for the pairs of *De* and *U* values chosen, we expect that the ratio of the magnitudes of the viscous terms (tending to disrupt the orientation distribution) and the molecular-elastic terms (tending to maintain the distribution in its equilibrium form) is approximately fixed. Let us denote the ratio of molecular-elastic to viscous terms by the fixed parameter Λ. Hence, for these points, we can think of steady state as being established when the magnitude of the gradient elasticity contributions in Eq. (3) is approximately equal to the *sum* of the viscous and molecular elasticity contributions, which is then, just $(1 + \Lambda)$ times the viscous terms. Therefore, apart from the factor Λ, which is a coefficient of order 1 or less (from calculations reported in Chaubal and Leal [18] we estimate $\Lambda \sim 0.3$), we should expect the Marrucci scaling to apply for the specific points chosen.

As mentioned before, the key aspects to monitor in the analysis of the results in this first part of the work are the evolution of the *director* (i.e. the major eigenvector of the configuration tensor) in the plane of shear, and the configuration profile across the gap. For all values of the parameters considered, the qualitative behavior of the system was the same, with only quantitative differences in the value of the emerging texture length scale (which we will discuss at the end of this section). Hence, we will present figures for only one set of parameters, namely $U = 8$, $De = 15$, $Er = 8 \times 10^6$, and homeotropic BCs. We chose this set only because it was in a central region of the range examined. The comments we will make apply to all other cases. The details of the other cases considered will be included in the Ph.D. thesis of Sgalari.

5.2. Results

Fig. 5 shows the evolution of the in-plane director orientation angle θ, i.e. the angle formed by the director and the positive *x* semi-axis at three different positions across the gap. We see that at all three points the director is initially tumbling. The apparent discontinuities in the angle at -90° are in fact only due to the definition of θ, which uses the fore-aft symmetry of the director. The director, in reality, keeps rotating in the same sense but as one end crosses the negative y semi-axis, $\theta = -90^\circ$, one has to switch to the opposite end which is appearing at $\theta = +90^\circ$. Initially, the directors rotate in unison, reflecting the constant shear rate across the gap, and the lack of any effect of distortional elasticity. As time progresses, however, the directors at the three points no longer rotate in synchrony, and then, one by one, they stop rotating altogether. After ~60 strain units (su), the director at all points throughout the gap only oscillates around the *x*-direction. We see, for example, that the director at $y \sim 0.6$ completes only one tumbling rotation, then oscillates around the flow direction before completing one additional tumbling cycle during the final part of the system transient. It may seem peculiar at first that the suppression of director tumbling should first occur at this intermediate point, rather than closer to the wall where the director orientation is fixed by the homeotropic anchoring condition. However, this is a consequence of the fact that director tumbling can be suppressed both due to the so-called "wind-up" effects of distortional elasticity (discussed further below), and to defocusing of the orientation distribution function. In particular, it is known from earlier studies of the monodomain Doi model that tumbling is arrested when the flow is strong enough to significantly reduce the degree of nematic alignment. Indeed, in the results shown in Fig. 5, the order in which the various points stop tumbling seems to be strongly dependent on the local value of the order parameter as will be discussed later.

Well-known previous works [31,32], done in the context of the LE theory, also predicted the suppression of tumbling in a sheared nematic. In the LE system, however, this was entirely due to the build-up of a gradient in the director orientation across the gap, a state that is known as "winding up" of the director field and is generated by tumbling itself. The mechanism for arrest of tumbling in this case is the resistance

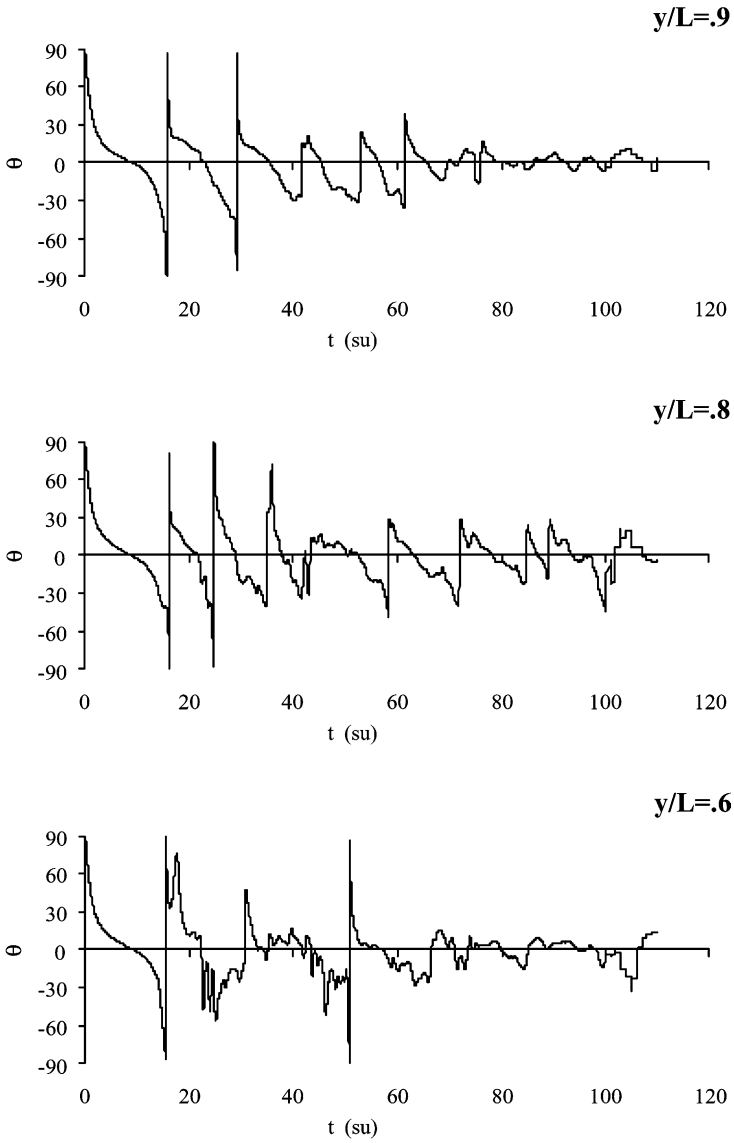

Fig. 5. Director in-plane angle vs. non-dimensional time (su) for three points at $x = 0$: $y/L = 0.9, 0.8, 0.6$. The parameter values are $U = 8$, $De = 15$, $Er = 8 \times 10^6$, with homeotropic BCs and an initial equilibrium orientation field.

to further build-up of this orientation gradient due to the action of distortional (i.e. Frank) elasticity. In our system, as already noted, the distortional elasticity due to gradients in the orientation angle is not the only mechanism responsible for the suppression of tumbling. If we look (Fig. 6) at the profile of the order parameter across the gap at different times, for the same case shown in Fig. 5, we see that as tumbling rotations are performed, the initially uniform order-parameter profile shows an increasing number of dips.

In the figure shown, the order parameter falls to values of $\sim$0.4 (the depth of the dips varies only slightly with the values of *De* and *Er*). We remind the reader that 0.53 is the value below which the model nematic

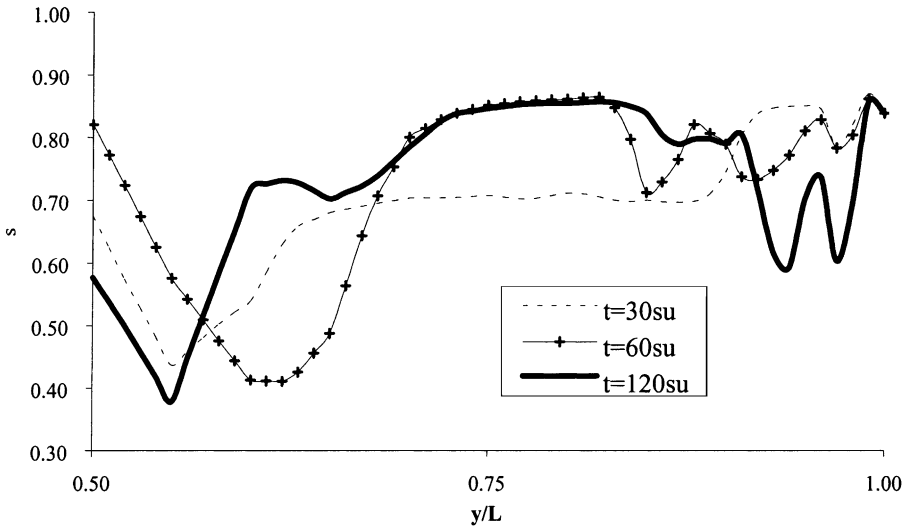

Fig. 6. Order parameter profile across the gap at $x = 0$ at three different times.

with distortional elasticity completely neglected becomes flow-aligning for all values of the shear rate (see Section IID of Marrucci and Greco [34]). Significantly, the tumbling first stops in Fig. 5 at the point, $y \sim 0.6$, where the first dip in the order parameter profile is formed. Finally, as a side comment, we note that the fact that the order parameter in those areas has a value considerably lower than the equilibrium value, justifies our original remark about the fact that the LE model will miss important physics, at least

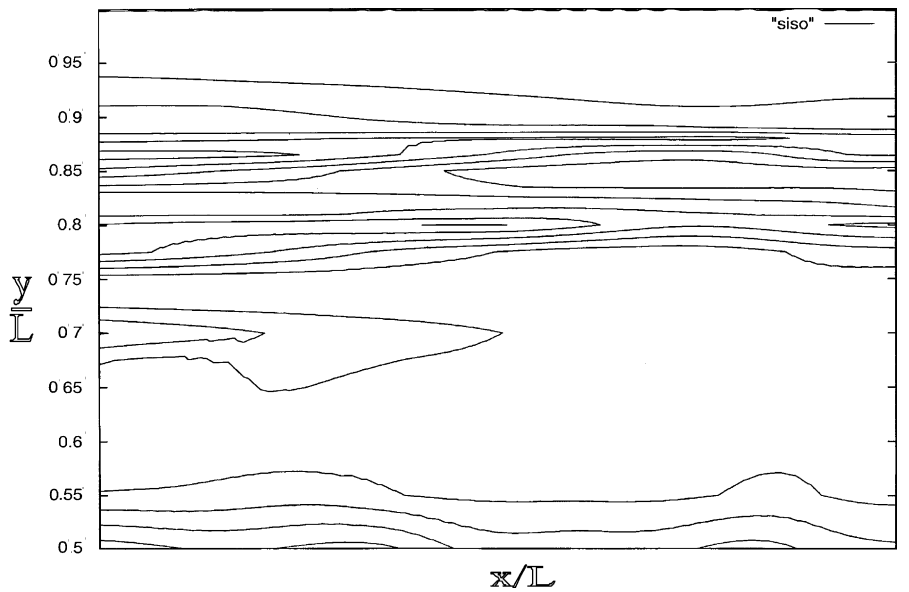

Fig. 7. Order parameter isolines at $t = 135$ su.

in this range of parameters. Clearly, the tumbling characteristics of the nematic cannot be described in this case with a constant (equilibrium) value for the order parameter.

When one looks at the full 2D geometry, it is found that the regions of decreased orientational order are roughly parallel to the flow direction as shown in Fig. 7. Even though a perfect identification is not possible, due to the lack of a full experimental picture of the configuration profile across the gap, we tentatively identify the area of the dips in s with the highly stretched (i.e. elongated in the flow direction) disclination loops predicted by Marrucci and Greco [34] that are characterized by a defect core in a "melted" state that is much less ordered than the bulk nematic phase (i.e. with a smaller order parameter). According to Marrucci and Greco [34] the mechanism for the suppression of tumbling, discussed before, may be envisioned as an "anchoring effect" on the orientation field due to these defect lines.

In Fig. 8a and b we plot the order parameter together with the orientation angle for the director at a particular moment in time. We see that the profile of the director orientation across the gap closely follows that of the order parameter. In particular, the orientation angle changes sign in the regions where the order

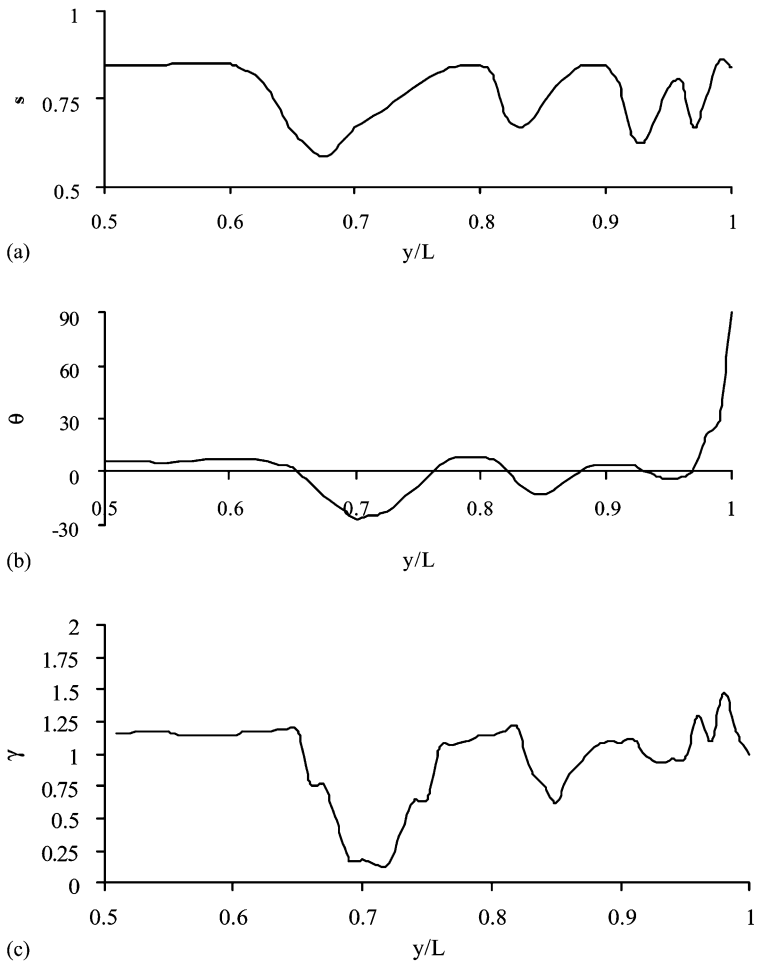

Fig. 8. Order parameter (a); tumbling angle (b); and velocity gradient (c) profiles across the gap at $x = 0$ at $t = 135$ su.

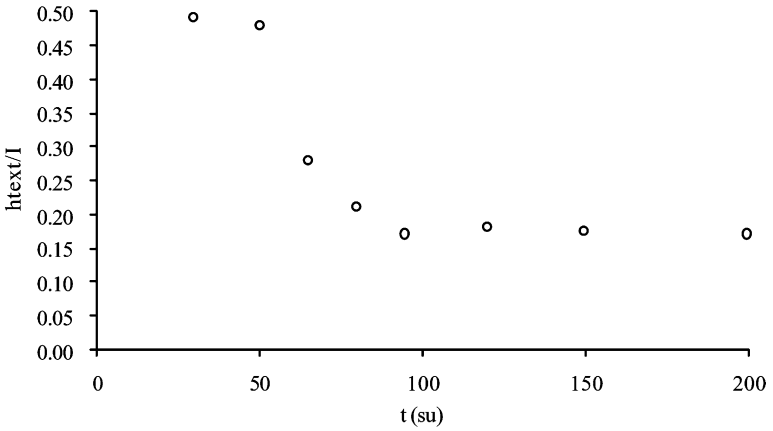

Fig. 9. Time evolution of texture length scale (Fourier spectra maximum of order parameter profile).

parameter is lower, while it attains its maximum values in the regions between the order parameter dips. This relation between the two profiles agrees with the theoretical predictions in Section IIIE of Marrucci and Greco [34].

For a complete physical understanding of these defect-like regions, it is useful to examine the velocity gradient profile across the gap at the time considered previously (Fig. 8a and c). In the regions that we have suggested as corresponding to disclinations, we see that the velocity gradient is locally reduced. This is not a surprise, since the viscosity strongly increases for lower values of the order parameter (since $\eta = \alpha kT/2\bar{D}_r$, one can see from Eq. (4) that $\eta \propto (1 - s^2)^2$). The defects then behave as obstacles to the overall flow, with a local reduction of the shear rate in those regions.

The qualitative description of the system evolution just presented, is complemented by a quantitative characterization of the texture. We looked, in particular, at the Fourier spectra of the order parameter profiles and analyzed their evolution in time. In Fig. 9 we plot the dominant length scale deduced from the Fourier analysis versus time. We see that, as tumbling is suppressed (around ∼60 su), the characteristic length scale starts to decrease. After ∼100 su, we can say that this length scale has become constant. Beyond this point, only minimal fluctuations (of order 0.01–0.02) are seen in the value of the dominant length scale, with significant changes occurring only in the short-scale secondary peaks of the Fourier spectrum, which correspond to the finer details of the profile. We note, in fact, that the configuration never reaches a completely stationary state, but the director keeps on oscillating around the flow direction and the disclinations oscillate slightly up and down across the gap.

Fig. 10 shows the dependence of the final steady texture scale h_{text} on the length scale l that is characteristic of distortional elasticity in the model. We see that, for the lower values of l/L, the data seem to fall on a straight line as expected from Eq. (10). For the largest value of l/L examined, the texture length scale appears in Fig. 10 to saturate. However, at this point, the texture scale has reached a value that is comparable to the half gap width (i.e. only one defect line is present in the system) and we do not expect the argument that led to Eq. (10) to hold in this case.

Kupfermann et al. [15] obtained comparable solutions in a recent investigation for a calculation that was strictly 1D. These authors also examined the dependence of the texture length scale calculated from their results on the length scale l of distortional elasticity. Surprisingly, in their work the texture

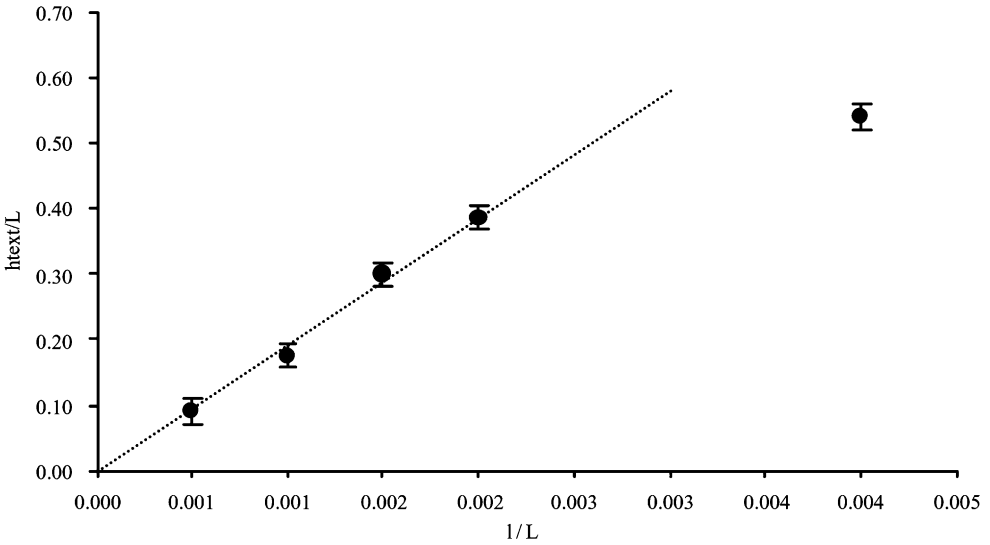

Fig. 10. Texture length scale vs. l/L for $U = 8$, $De = 15$ (error bars are indicative of the magnitude of the time fluctuations in the value of the Fourier spectra maximum).

scale did not exhibit the expected scaling. The reason for the discrepancy between their results and ours on this point is unclear. We can offer only some possible speculations. First of all, they studied a low dimensional system: in their calculation they considered only 1D flow without any x dependence of the various quantities, and a strictly 2D configuration tensor. Another possibility is that they used the quadratic closure in their simulations. Even though they preserve tumbling behavior because of the choice of finite aspect ratio for the rod-like molecules in their model, it is known [27] that the viscous term, an essential element in the force balance, is not well approximated by this choice of closure. Thirdly, they did not retain the dependence of the rotational diffusivity on the local configuration (Eq. (4)), assuming instead a

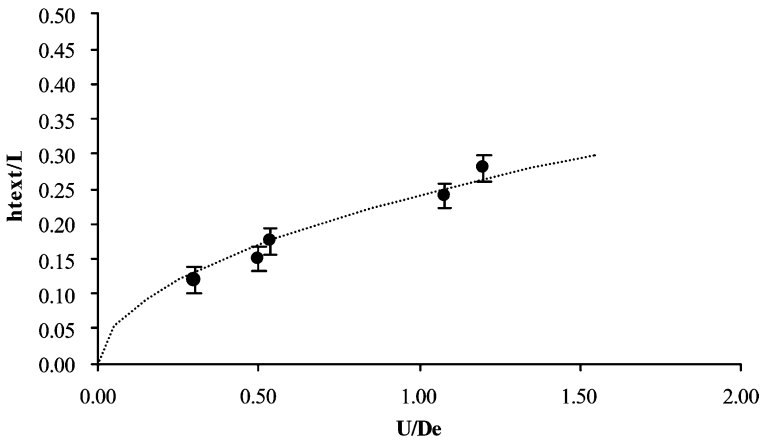

Fig. 11. Texture length scale vs. U/De for $l/L = 0.001$.

constant value throughout the gap. Considering the strong effect that variations in the value of the order parameter have on the actual diffusivity, their simplifying assumption could lead to serious inaccuracies, especially in regions with strongly varying degree of order (i.e. near defects). Finally, they studied systems characterized by much lower values of the Ericksen number ($O(10^2)$) than our work ($O(10^6)$). May be, in that area of parameter space, the Marrucci scaling simply does not apply. In any case it is gratifying that this aspect of the expected scaling argument does appear to be verified by the present calculations.

Finally, in Fig. 11 we plot the dependence of the texture length scale on the ratio U/De. According to Eq. (10), this should be expected to vary as $(U/De)^{1/2}$, and we see that a 1/2 power fitting roughly captures the trend of our data. It should be noted, however, that the error bars on these points (as in Fig. 10, these error bars represent the magnitude of the temporal fluctuations in the value of the maximum of the Fourier spectrum) are large enough that they could also have been fitted with a linear dependence on U/De. We stress, moreover, that our data were obtained by examining specific pairs of values for De and U. The relation between h_{text} and U/De indicated by Eq. (10) is, as we have said, not expected to hold for the general case when molecular elasticity (viscoelasticity) is included in the model, as in the present work.

6. Part II: uncostranied configuration tensor

6.1. Objective and general remarks

As noted in the introduction, previous computational studies using the LE theory [6–8] have already predicted an evolution of the system with director tipping or with the formation of roll cells aligned in the flow direction [9] leading to a striped director field. Even though there are still some qualitative discrepancies between the experimental observations and the fine details of the texture predicted theoretically, there is general agreement that the physical picture of rolls cells as being responsible for the flow-aligned striped texture is the correct one. As long as the present simulations are limited to a 2D flow, we would not be able to predict this final texture, as already noted.

Instead, by releasing the constraint of a configuration tensor that is symmetric with respect to the shear plane, we hope to obtain predictions for the configuration field that can be somehow related to the banded texture perpendicular to the flow direction that arises before the inception of the roll cells. We remind the reader that the earlier analysis of the banded structure, due to Han and Rey [8], considered only low values of the shear rates, i.e. values for which the basic assumptions of the LE theory they used are valid. So our calculations are aimed at extending their results to the regime of higher De and Er.

As in Section 5, we will show results only for one set of parameter values $U = 8$, $De = 15$ and $Er = 8 \times 10^6$, but we will consider all types of BC: homeotropic, parallel and alignment in the vorticity direction.

6.2. Results

The most significant result of our calculations is that small perturbations ($O(10^{-4})$), either uniform or sinusoidal in space, and either in the bulk or in the anchoring angles, were sufficient to trigger an out-of-plane instability for both homeotropic and parallel anchoring. As seen in experiments, our simulations predict that, for both types of initial and anchoring configurations, the director tips out of the shear plane after an initial transient period of tumbling in the shear plane that depends on whether we have

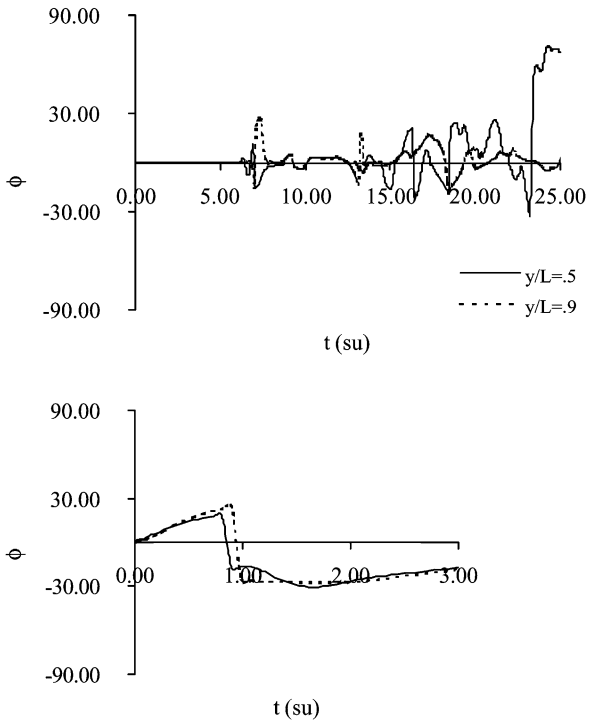

Fig. 12. Director out-of-plane angle vs. time for two points at $x = 0$, for the two anchoring conditions: (a) homeotropic; (b) parallel.

parallel or homeotropic anchoring. Plotted in Fig. 12 is the evolution of the out-of-plane angle φ for two points across the gap for the two types of BCs. We see that significant tipping occurs after 15–20 su (a time that corresponds to ∼1 tumbling period) for the case of homeotropic anchoring. In contrast, only ∼1 su is needed for tipping in the case of parallel BC. This difference in the time scale for director tipping is similar to the difference in the time scale required for the system to show bands that we observe in our simulations, as will be discussed later, and similar to the difference in the time scale for band evolution in real experiments (see Fig. 1).

Looking at the configuration profile across the gap we still see a modulation in the magnitude of the order parameter (as was also true in the preceding section) but here we also see a non-uniformity in the out-of-plane angle. For a compact representation of the complete variation of the configuration across the gap, a convenient format is the "ribbon plot" shown in Fig. 13. The orientation of the director in the upper half of the gap (at $x = 0$ and at two different times $t = 12$ and 18 su for the case of homeotropic anchoring) is represented by the orientation of the rods, while the value of the order parameter at different positions is indicated by the length of the rods. Evident is the progressive twist in the ribbon toward out-of-plane orientations (i.e. the out-of-plane tipping shown by the two points of Fig. 12 is a trend present throughout the gap). We also note that the characteristic magnitude of the order parameter modulation is comparable to that of Section 5 for profiles obtained at the same time.

As the available *experimental* images of the texture evolution of actual LCPs are based on patterns of polarized light transmitted onto the bottom plane of the shear cell, a comparison between theory and

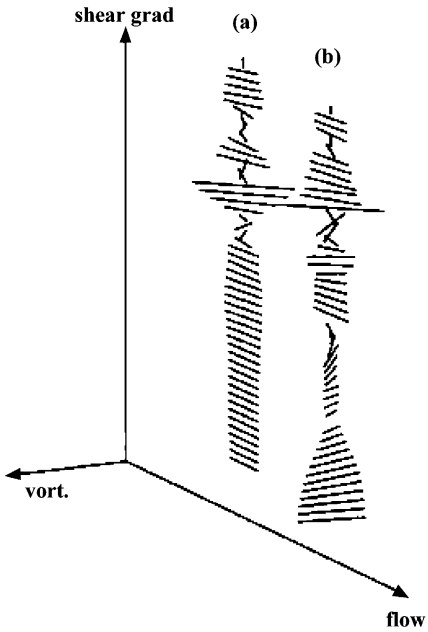

Fig. 13. Configuration profile in the upper half of the gap at $x = 0$, for homeotropic BC at $t = 12$ su (a); and at $t = 18$ su (b).

experiments requires that we compute what the transmitted light profiles would look like in our systems. We imagine that polarized light is shone across the gap and, after having interacted with the non-uniform configuration field, it is viewed on the bottom plane through a crossed polarizer. To obtain the profile of the transmitted light intensity we generalized a computational procedure originally developed by Han and Rey [8] to the case of nematic with non-uniform order parameter (and therefore non-uniform local birefringence). For either type of BC, we find that non-uniformities in the transmitted light intensity profile develop on the same timescale as the first significant out-of-plane tipping of the director (see Fig. 14 for homeotropic BC). We are tempted to identify these non-uniformities with the appearance of

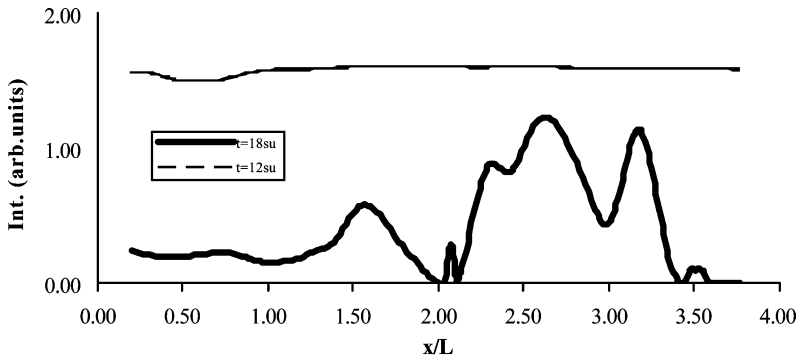

Fig. 14. Transmitted light profile for homeotropic BC at $t = 12$ and 18 su.

bands perpendicular to the flow direction in real sheared systems. However, due to the limited dimensions of the slab considered, and the fact that no z dependence is assumed, unequivocal verification is, at the moment, not possible on this issue.

Finally we find, for wall anchoring in the vorticity direction, that all small perturbations in the anchoring angles or in the ICs are quickly dampened out and that the uniform configuration is the stable solution. This agrees with what is seen in the Larson–Mead experiments (see Fig. 1): no banded pattern forms.

6.3. Discussions

The out of plane tipping of the director had already been predicted in previous theoretical works, both in the LE context [6–8] and in the original Doi formulation [18,33]. In the first series of works, the force driving this instability was the windup of the director orientation created by tumbling as discussed in Section 5. In contrast, in the original Doi theory [18,33], pure viscoelastic effects due to molecular elasticity were sufficient to destabilize the in-plane tumbling and make the vorticity direction a stable attractor. Our work, for the first time, takes into account both effects in the 3D evolution of the orientation distribution and it represents, therefore, the first realistic prediction for high values of the *Er*. Interestingly, some of the qualitative aspects of the LE solutions, which, as we said, are valid only for low values of the *Er*, are preserved in our results. For example, the "twisted ribbon" profile of the director across the gap, and the appearance of non-uniformities in the transmitted light profile, are similar to what was found by Han and Rey [6–8], using the LE approximation. We note, however, that the texture they obtained is much coarser than the one we found because of the low shear rates they considered.

Comparing with the texture evolution of real materials, we see that our predictions can qualitatively capture the out-of-plane tipping of the director, and also appear to reflect the difference in time scale for this instability to take place when going from homeotropic to parallel BCs, that was seen in the Larson–Mead experiments.

7. Conclusions

The numerical scheme developed in this work for implementation of the Marruci–Greco version of the Doi theory for LCPs with distortional elasticity was shown to be capable of predicting a texture evolution in shear flows. Moreover, even in the simplest approximation of the model, with the assumption of a symmetric distribution about the shear plane, the characteristic length scale of the emerging texture was found to respect expected scalings.

Upon releasing the constraint of a configuration tensor that is symmetric with respect to the plane of shear, we found that in-plane solutions are unstable to out-of-plane tipping and that the resulting configuration field is no longer uniform along the flow direction. This is in qualitative agreement with what is observed in experiments. The order of magnitude of the time scale for the tipping instability is comparable to experimental values for typical LCP solutions.

Unfortunately no experimental images are available of the configuration profile across the gap, and thus, a complete verification of the present results is not yet possible. We hope that improvements in experimental techniques may soon produce data of this type.

In conclusion, our model has shown promising predictive capabilities even though, to fully test its potential for the prediction of LCP texture evolution, we will need to remove the 2D-flow assumption. In

fact only 3D flow calculations will allow for roll-cell formation and the striped texture that characterizes the final steady state of actual LCP materials. Such calculations are currently in progress.

Acknowledgements

Calculations were performed on AMD 600 computers at the MRL Central Facilities supported by the National Science Foundation under award No. DMR96-32716. G.S. was supported by a grant from the Petroleum Research Fund. J.J.F. was partly supported by a 3M Non-Tenured Faculty Award, a PSC-CUNY research grant and an NSF Career Award.

References

[1] R.G. Larson, D.W. Mead, Development of orientation and texture during shearing of liquid crystalline polymers, Liquid Cryst. 12 (1992) 751–768.
[2] R.G. Larson, D.W. Mead, The Ericksen number and the Deborah number cascades in sheared polymeric nematics, Liquid Cryst. 15 (1993) 151–169.
[3] K. Hongladarom, W.R. Burghardt, Molecular alignment of polymer liquid crystals in shear flows. 2. Transient flow behavior in poly(benyilglutamate) solutions, Macromolecules 26 (1993) 772–784.
[4] J. Vermant, P. Moldenaers, S.J. Picken, J. Mewis, A comparison between texture and rheological behavior of lyotropic liquid crystalline polymers during flow, J. Non-Newt. Fluid Mech. 53 (1994) 1–23.
[5] N.X. Yan, M.M. Labes, Critical behavior of shear-induced transient periodic structures in a liquid crystalline polymer as a function of molecular weight, Macromolecules 27 (1994) 7843–7845.
[6] W.H. Han, A.D. Rey, Supercritical bifurcations in simple shear flow of a non-aligning nematic: reactive parameters and anchoring effects, J. Non-Newt. Fluid Mech. 48 (1993).
[7] W.H. Han, A.D. Rey, Simulations and validation of nonplanar nematorheology, J. Rheol. 38 (1994) 1317–1318.
[8] W.H. Han, A.D. Rey, Theory and simulation of optical banded textures of nematic polymers during shear flow, Macromolecules 28 (1995) 8401–8405.
[9] J. Feng, J. Tao, L.G. Leal, Roll cells and disclinations in sheared polymer nematics, J. Fluid Mech. 449 (2001) 179–200.
[10] P.T. Mather, D. Pearson, R.G. Larson, Flow patterns and disclination-density measurements in sheared neamtic liquid crystals, Liquid Cryst. 20 (1996) 527–538.
[11] R.G. Larson, M. Doi, Mesoscopic domain theory for textured liquid crystalline polymers, J. Rheol. 35 (1991) 539.
[12] G. Marrucci, F. Greco, The elastic constants of Maier–Saupe rod-like molecule nematics, Mol. Cryst. Liquid Cryst. 206 (1991) 17–30.
[13] J. Feng, G. Sgalari, L.G. Leal, A theory for flowing nematic polymers with orientational distortions, J. Rheol. 44 (2000) 1085–1101.
[14] T. Tsuji, A.D. Rey, Effect of long-range order on sheared liquid crystalline materials. I. Compatibility between tumbling behavior and fixed anchoring, J. Non-Newt. Fluid Mech. 65 (1996) 269–289.
[15] R. Kupfermann, M.N. Kawaguchi, M.M. Denn, Emergence of structure in a model of liquid crystalline polymers with elastic coupling, J. Non-Newt. Fluid Mech. 91 (2000) 255–271.
[16] G. Marrucci, The rheology of liquid crystalline polymers, Pure Appl. Chem. 57 (1985) 1545.
[17] M. Doi, Molecular dynamics and rheological properties of concentrated solutions of rod-like polymers in isotropic and liquid crystalline phase, J. Polym. Sci., Polym. Phys. Ed. 19 (1981) 229–243.
[18] C.V. Chaubal, L.G. Leal, Smoothed particle hydrodynamics techniques for the solution of kinetic theory problems. 2. The effect of flow perturbations on the simple shear behavior of LCPs, J. Non-Newt. Fluid Mech. 82 (1999) 25–55.
[19] H.C. Ottinger, Time-structure invariance criteria for closure approximations, Phys. Rev. E 56 (1997) 4097–4103.
[20] M. Van Gurp, On the use of the spherical tensors and the maximum entropy method to obtain closure for anisotropic fluids, J. Rheol. 39 (1995) 73.
[21] M. Doi, S.F. Edwards, The theory of Polymer Dynamics, 1986.

[22] J. Feng, L.G. Leal, Pressure driven channel flows of a model liquid crystalline polymer, Phys. Fluid 11 (1999) 2821–2835.
[23] D. Doraiswamy, A.B. Metzner, The rheology of polymeric liquid crystals, Rheol. Acta 25 (1986) 580–587.
[24] N. Mori, Y. Tsuji, K. Nakamura, C. Yoshikawa, Numerical simulations of the flow of liquid crystalline polymers between parallel plates containing a cylinder, J. Non-Newt. Fluid Mech. 56 (1995) 85–97.
[25] P. Singh, L.G. Leal, Finite element simulations of the start-up problem for a viscoelastic fluid in an eccentric rotating cylinder geometry using a third order upwind scheme, J. Non-Newt. Fluid Mech. 58 (1995) 279–313.
[26] J. Feng, L.G. Leal, Simulating complex flows of liquid crystalline polymers using the Doi theory, J. Rheol. 41 (1997) 1317–1335.
[27] J. Feng, C.V. Chaubal, L.G. Leal, Closure approximations for the Doi theory: which to use in simulating complex flows of liquid crystalline polymers? J. Rheol. 42 (1998) 1095–1119.
[28] M.J. Szady, T.R. Salamon, A.W. Liu, D.E. Bornside, R.C. Armstrong, R.A. Brown, A new mixed finite element method for viscoelastic flows governed by differential constitutive equations, J. Non-Newt. Fluid Mech. 59 (1995) 215–243.
[29] D.D. Joseph, J.C. Saut, Change of type and loss of evolution in the flow of viscoelastic liquids, J. Non-Newt. Fluid Mech. 20 (1986) 117–141.
[30] F.P.T. Baajens, Mixed finite element methods forviscoelastic flow analysis: a review, J. Non-Newt. Fluid Mech. 79 (1998) 361–385.
[31] P. Manneville, The transition to turbulence in nematic liquid crystals, Mol. Cryst. Liquid Cryst. 70 (1981) 223.
[32] T. Carlsonn, Theoretical investigation of the shear flow of nematic liquid crystals with the Leslie viscosity $\alpha_3 > 0$: hydrodynamic analogue of first order transition, Mol. Cryst. Liquid Cryst. 104 (1984) 307.
[33] R.G. Larson, H.C. Ottinger, Effect of molecular elasticity on out-of-plane orientations in shearing flows of liquid crystalline polymers, Macromolecules 24 (1991) 6270–6282.
[34] G. Marrucci, F. Greco, Flow behavior of liquid crystalline polymers, Adv. Chem. Phys. 86 (1994) 331–404.